Journal of Microscopy and Ultrastructure 4 (2016) 133–142

Contents lists available at ScienceDirect

Journal of Microscopy and Ultrastructure

journal homepage: www.elsevier.com/locate/jmau

Original Article

Histological study on the protective effect of endogenous stem-cell mobilization in Adriamycin-induced chronic nephropathy in rats

Eman Mostafa Sadek, Nagla Mohamed Salama, Dalia Ibrahim Ismail*, Asmaa Ahmed Elshafei

Histology Department, Faculty of Medicine, Cairo University, Cairo, Egypt

ARTICLE INFO

Article history:
Received 27 September 2015
Received in revised form
28 November 2015
Accepted 25 December 2015
Available online 31 December 2015

Keywords:
adriamycin
caspase-3
CD34
chronic kidney disease
granulocyte colony-stimulating factor

ABSTRACT

Chronic kidney disease is a global health problem with increasing morbidity and mortality. Therefore, this study was planned to test the protective effect of hematopoietic-stem-cell mobilization by granulocyte colony-stimulating factor (G-CSF) on Adriamycin (ADR)-induced chronic renal disease in rats. Thirty albino rats were equally divided into three groups: control, ADR group [rats received a single intravenous injection of ADR (5 mg/kg)], and G-CSF group [rats received ADR by the same route and the same dose as the previous group, and then G-CSF (70 μg/kg/d) 2 hours after ADR injection then daily for five consecutive days]. At the time of sacrifice (after 6 weeks), blood samples were taken to estimate the blood urea nitrogen and serum creatinine. Kidney sections were stained with hematoxylin and eosin, toluidine blue, Masson's trichrome, periodic acid–Schiff stains, and immunohistochemical staining against CD34 and caspase-3. The G-CSF group exhibited protection against renal injury manifested by reducing blood urea nitrogen and serum-creatinine levels, improving histological architecture, and increasing the proliferative capacity of renal tubules.

© 2015 Saudi Society of Microscopes. Published by Elsevier Ltd. All rights reserved.

1. Introduction

Chronic kidney disease (CKD) is a public worldwide health problem. It causes many complications, and it has become an important research field because of its increasing morbidity and mortality [1].

Infusion of stem cells was reported to contribute toward tubule regeneration following acute or chronic renal failure [2]. However, recent studies have suggested that the primary means of repair by these cells involves paracrine and endocrine effects, rather than direct stem-cell differentiation into damaged tubules [3].

Homing factors can be beneficial to damaged tissue, as they stimulate the migration of hematopoietic and mesenchymal stem cells [4]. Among the homing factors, granulocyte colony-stimulating factor (G-CSF) is known to mobilize hematopoietic stem cells (HSCs) from bone marrow (BM) to peripheral circulation. Its protective action on renal function has been demonstrated in mouse models of acute renal failure; however, there have been few investigations on its role in CKD [2].

The aim of this study was to evaluate the protective effect of HSC mobilization by G-CSF in a rat model of Adriamycin (ADR)-induced CKD, monitored by histological, morphometric, and serological methods.

* Corresponding author. Histology Department, Kasr Alainy Faculty of Medicine, Cairo University, 4, Alfalaky street, Kasr Alainy, Cairo, Egypt.
E-mail address: drdaliaibrahim@hotmail.com (D.I. Ismail).

http://dx.doi.org/10.1016/j.jmau.2015.12.003
2213-879X/© 2015 Saudi Society of Microscopes. Published by Elsevier Ltd. All rights reserved.

2. Materials and methods

2.1. Materials

2.1.1. Drugs

Doxorubicin hydrochloride (ADR) was purchased in the form of vials (50 mg/25-mL saline) from EIMC United Pharmaceuticals (EUP), Badr City, Cairo, Egypt.

G-CSF (Neupogen) was provided in the form of prefilled syringes of 0.5 mL containing 30 million units (= 300 μg) of filgrastim (recombinant methionyl human G-CSF, r-metHuG-CSF, from *Escherichia coli* K12) (F. Hoffmann-La Roche Ltd., Basel, Switzerland/Kirin-Amgen Inc., Basel, Switzerland).

2.1.2. Animals

This study included 30 adult male albino rats about 12 weeks old, with an average body weight of 180–200 g. The animals were provided with veterinary care by the Animal House of Faculty of Medicine, Cairo University, Cairo, Egypt, according to the guidelines for animal research approved by the Animal Ethics Committee, Faculty of Medicine, Cairo University. They were caged in a conventional clean facility at 22–26 °C, and allowed food and water *ad libitum*. The rats were equally divided into three groups of 10 rats each.

In Group I (control group), the rats were subdivided into (1) Subgroup IA, in which five rats received a single intravenous injection (tail vein) of 0.5-mL saline; and (2) Subgroup IB, in which five rats received a single intravenous injection (tail vein) of 0.5-mL saline, and then subcutaneously received 0.5-mL glucose 5% after 2 hours then daily for 5 consecutive days.

In Group II (ADR group), the rats received a single intravenous injection (tail vein) of ADR at a dose of 5 mg/kg of body weight [5].

In Group III (G-CSF group), the rats received ADR by the same route and the same dose as the previous group, and then G-CSF was given 2 hours after the ADR injection. G-CSF was subcutaneously injected daily for 5 consecutive days at a dose of 70 μg/kg/d diluted in 0.5-mL glucose 5% [6].

Three rats from each group were sacrificed after 5 days from the beginning of the experiment by intraperitoneal injection of pentobarbital sodium 60 mg/kg [7], while the remaining rats were sacrificed in the same way 6 weeks after the beginning of the experiment.

2.2. Methods

2.2.1. Laboratory investigations

At the time of sacrifice (6 weeks), blood samples were taken from the retro-orbital vein into heparinized tubes, and transferred to the Biochemistry Department, Faculty of Medicine, Cairo University, to detect the levels of blood urea nitrogen (BUN) and serum creatinine to assess the kidney function.

2.2.2. Histological examination

Kidney specimens from rats sacrificed after 5 days were collected, processed, and immunostained with anti-CD34 antibody to assess the mobilization and homing of HSCs into the kidney [8].

Kidney specimens from rats sacrificed at the end of the experiment (after 6 weeks) were collected. (1) Right-kidney specimens were fixed in 10% buffered formalin, and then paraffin embedded. Serial sections of 5–7 μm thickness were cut, and subjected to (i) hematoxylin-and-eosin (H&E) stain [9]; (ii) Masson's trichrome stain to demonstrate collagen fibers [9]; (iii) periodic acid–Schiff (PAS) reaction [9] to demonstrate basal lamina and brush border as a measure of tubular injury; (iv) immunohistochemical staining using anti-CD34 antibody, which is a ready-to-use mouse monoclonal antibody (Dako, Glostrup, Denmark), to demonstrate HSCs [8], and positive cells showed a membranous/cytoplasmic brown reaction; and (v) immunohistochemical staining using anticaspase-3 antibody, which is a ready-to-use rabbit polyclonal antibody (Thermo Scientific Laboratories, Neo Markers, Waltham, Massachusetts, USA), to demonstrate apoptosis [8], and caspase-3 marker shows cellular cytoplasmic localization in early apoptosis and nuclear localization in late apoptosis [10]. (2) Left-kidney specimens (about 1 mm) were processed for embedding in epoxy resin. Semithin sections were cut at 1-μm thickness, and rapidly fixed in 3% phosphate-buffered glutaraldehyde, stained with toluidine blue, and then examined by a light microscope [11].

2.2.3. Morphometric study

Data were obtained using Leica QWin 500 C image analyzer computer system (Leica Microsystems, Cambridge, England, UK). The following were measured: (1) number of affected Malpighian corpuscles per low-power field (100 ×) in H&E-stained sections (widening of Bowman's space, partial or complete destruction, loss of glomerular tufts) [12]; (2) area percent of collagen in Masson's trichrome-stained sections; (3) optical density of PAS +ve reaction; (4) number of CD34-immunopositive cells per low-power field; and (5) number of caspase-3-immunopositive cells per low-power field.

2.2.4. Statistical analysis

The measurements obtained were analyzed using SPSS software version 13 (SPSS Inc., Chicago, IL, USA). A comparison between the different groups was made using analysis of variance, followed by *post hoc* Tukey test. The results were expressed as means ± standard deviation. The differences were considered statistically significant when $p < 0.05$.

3. Results

3.1. Results of laboratory investigations

Laboratory investigation results are illustrated in Table 1.

3.2. Histological results

3.2.1. H&E-stained sections

Renal sections from both control subgroups (IA and IB) revealed normal histological architecture; the renal

Table 1
Mean values of blood urea nitrogen and serum creatinine ± standard deviation.

Groups	Blood urea nitrogen (mg/dL)	Serum-creatinine level (mg/dL)
I (control)	37.93 ± 1.36	0.13 ± 0.03
II (ADR)	91.77 ± 1.99 [a]	1.63 ± 0.20 [b]
III (G-CSF)	52.60 ± 1.13 [a,c]	0.66 ± 0.80

[a] Significant increase compared to Group I.
[b] Significant increase compared to both Groups I and III.
[c] Significant decrease compared to Group II.
ADR = Adriamycin; G-CSF = granulocyte colony-stimulating factor.

corpuscle appeared formed of tuft of glomeruli and Bowman's space. Proximal convoluted tubules showed narrow lumina, and were lined with high cuboidal cells with rounded basal nuclei and deeply acidophilic cytoplasm. Diatal convoluted tubules showed wider lumina, and were lined with cubical cells with rounded central nuclei and paler acidophilic cytoplasm (Figure 1A). The renal medulla showed normal histological architecture of the medullary collecting tubules that appeared lined with simple cuboidal epithelium with central rounded nuclei and pale acidophilic cytoplasm (Figure 1B).

Sections from Group II (ADR group) showed many forms of cortical and medullary affection. The cortex showed partial or complete destruction of a large number of renal corpuscles with loss of glomerular tufts. Most of the lining cells of the cortical tubules showed cytoplasmic vacuolation and pyknotic nuclei with cellular debris in the lumina (Figure 2A). Some cortical tubules exhibited dilatation with dense acidophilic hyaline casts in their lumina, as well as shedding and desquamation of their lining epithelium (Figure 2B). Other cortical sections showed marked interstitial hemorrhage and distorted glomeruli with widening of Bowman's spaces (Figure 2 C). Peritubular cellular infiltration was also seen (Figure 2D). The renal medulla revealed marked vascular capillary congestion. Many tubules showed desquamated epithelial cells, which appeared as cellular debris in the lumina. The lining tubular cells exhibited cytoplasmic vacuolation and pyknotic nuclei (Figure 2E).

Sections from Group III (G-CSF group) showed that most renal corpuscles appeared normal with intact glomerular tufts. Mild peritubular capillary congestion was noted with mild cytoplasmic vacuolation in some tubular cells. Nearly all tubular cells had vesicular nuclei (Figures 3A and 3B). Sections in the medulla showed that some collecting tubules contain cellular debris or mild cytoplasmic vacuolation (Figure 3C).

3.2.2. *Toluidine-blue-stained sections*

Sections from both control subgroups (IA and IB) showed apparently normal renal corpuscles with narrow Bowman's space. The renal tubules had clear basal striations, prominent brush borders, and large vesicular nuclei with prominent nucleoli, as well as clear continuous basal laminae (Figure 4A). Most renal tubules from the ADR group showed cytoplasmic vacuolation, nonclear basal striations, partial or complete loss of brush border, as well as many small irregular nuclei. Epithelial desquamation and interrupted basal laminae were also seen (Figure 4B). Renal tubules from the G-CSF group showed clear basal striations, prominent brush border, and large vesicular nuclei. However, mild cytoplasmic vacuolation and irregular nuclei were detected in some cells (Figure 4C).

3.3. *Histochemical results*

3.3.1. *Masson's trichrome-stained sections*

Sections from both control subgroups (IA and IB) revealed the same findings. The renal cortex showed the normal distribution of collagen, which appeared as fine collagen fibers among glomerular capillaries and between the renal tubules (Figure 5A). Renal cortex from Group II (ADR group) showed marked deposition of collagen fibers within the glomeruli in the renal corpuscles, as well as between the renal tubules (Figures 5B and 5C). As for Group III (G-CSF group), there was mild deposition of collagen fibers in the renal corpuscle and between the renal tubules (Figure 5D).

3.3.2. *PAS-stained sections*

The examined renal cortex from both control subgroups (IA and IB) showed multiple tubules with intact brush

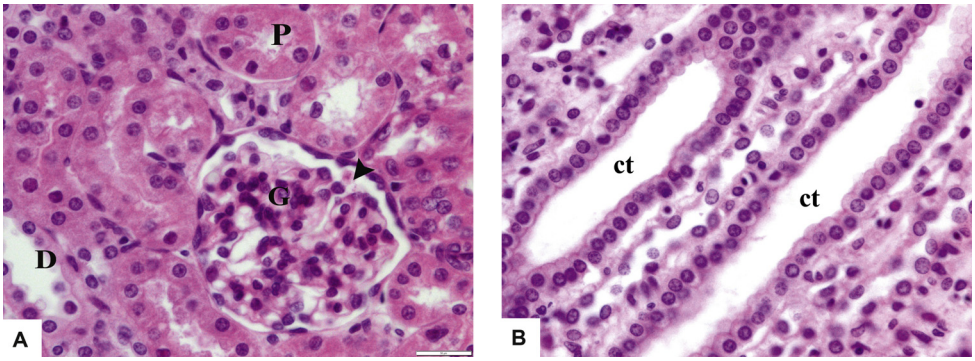

Fig. 1. Photomicrographs of renal sections from Group I (control group) stained with hematoxylin and eosin 400×. (A) The renal cortex shows Malpighian renal corpuscle containing glomerulus (G) and Bowman's space (arrowhead). The proximal convoluted tubules (P) have narrow lumina and are lined with high cuboidal cells with rounded vesicular basal nuclei and deeply acidophilic cytoplasm. The distal convoluted tubules (D) have wider lumina and are lined with cubical cells with rounded vesicular central nuclei and paler acidophilic cytoplasm. (B) The renal medulla shows collecting tubules (ct) lined with simple cuboidal epithelium with central rounded nuclei and acidophilic cytoplasm.

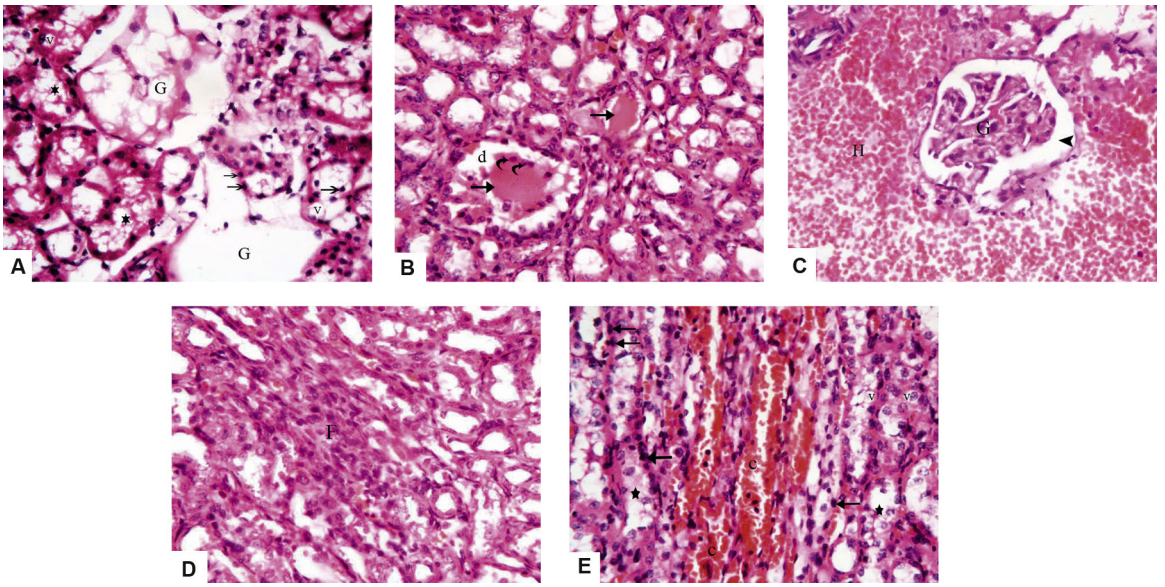

Fig. 2. Photomicrographs of sections from Group II (Adriamycin group) stained with hematoxylin and eosin 400×. (A) The cortex reveals complete destruction of the renal corpuscles with loss of glomerular tufts (G), the tubular lining cells show vacuolated cytoplasm (v) and pyknotic nuclei (arrows), and most tubular lumina contain cellular debris (stars). (B) There is dilatation (d) of some cortical tubules, dense acidophilic hyaline casts in their lumina (arrows) with shedding and desquamation of the lining epithelium (curved arrows). (C) Marked interstitial hemorrhage (H) is noticed, with distorted glomerulus (G) and widening of Bowman's space (arrowhead). (D) A heavy interstitial inflammatory infiltration (F) is present in the renal cortex. (E) The renal medulla shows marked vascular congestion (c), the tubular cells exhibit pyknotic nuclei (arrows), vacuolated cytoplasm (v) with cellular debris in tubular lumina (stars).

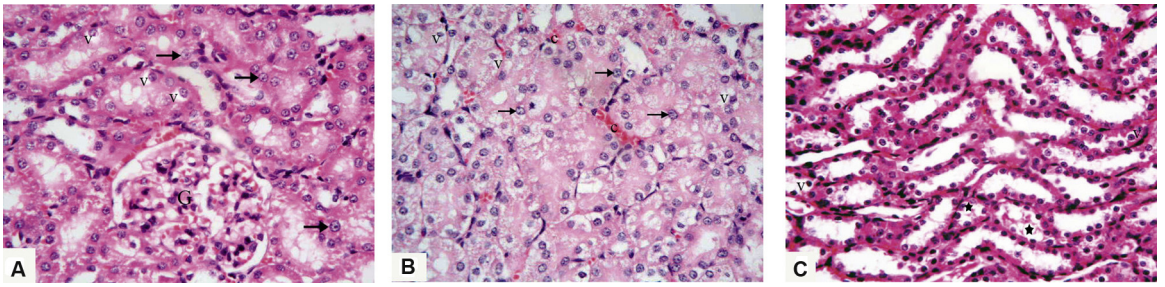

Fig. 3. Photomicrographs of renal sections from Group III (granulocyte-colony-stimulating-factor group) stained with hematoxylin and eosin 400×. (A) The renal cortex shows apparently normal renal corpuscle with glomerular tuft (G), few tubular cells show cytoplasmic vacuoles (v), and nearly all tubular cells have vesicular nuclei (arrows). (B) There is mild peritubular capillary congestion (c), cytoplasmic vacuolation (v) of some lining tubular cells, and almost all cells have vesicular nuclei (arrows). (C) The renal medulla reveals some collecting tubules contain cellular debris (stars) or mild cytoplasmic vacuolation (v).

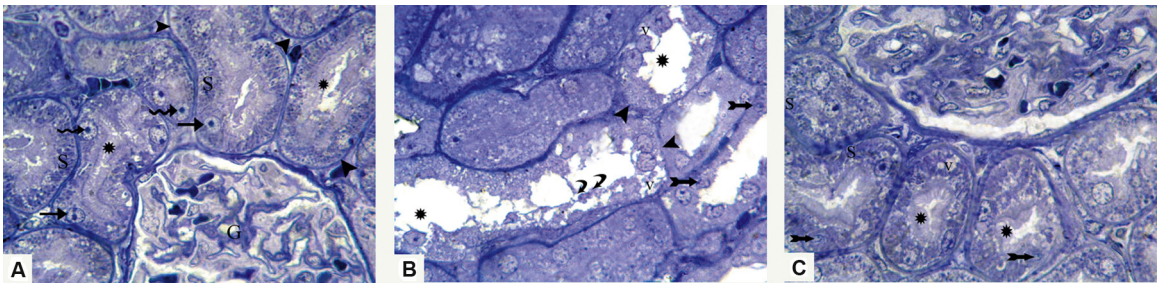

Fig. 4. Photomicrographs of semithin sections stained with toluidine blue 1000×. (A) Renal section from Group I (control group) shows part of apparently normal renal corpuscle containing a glomerulus (G); the renal tubular cells have clear basal striations (S), prominent brush borders (asterisks), large vesicular nuclei (arrows) with prominent nucleoli (spiral arrows), and clear basal laminae (arrowheads). (B) In sections from Group II (Adriamycin group), most renal tubules have cytoplasmic vacuoles (v), nonclear basal striations, partial or complete loss of brush border (asterisks), small irregular nuclei (bifid arrows), as well as desquamated cells (curved arrows), and the tubular basal laminae are interrupted at many sites (arrowheads). (C) Most renal tubules in Group III (granulocyte-colony-stimulating-factor group) show clear basal striations (S) and prominent brush border (asterisks). However, mild cytoplasmic vacuolation (v) and irregular nuclei (bifid arrows) appear in some tubular cells.

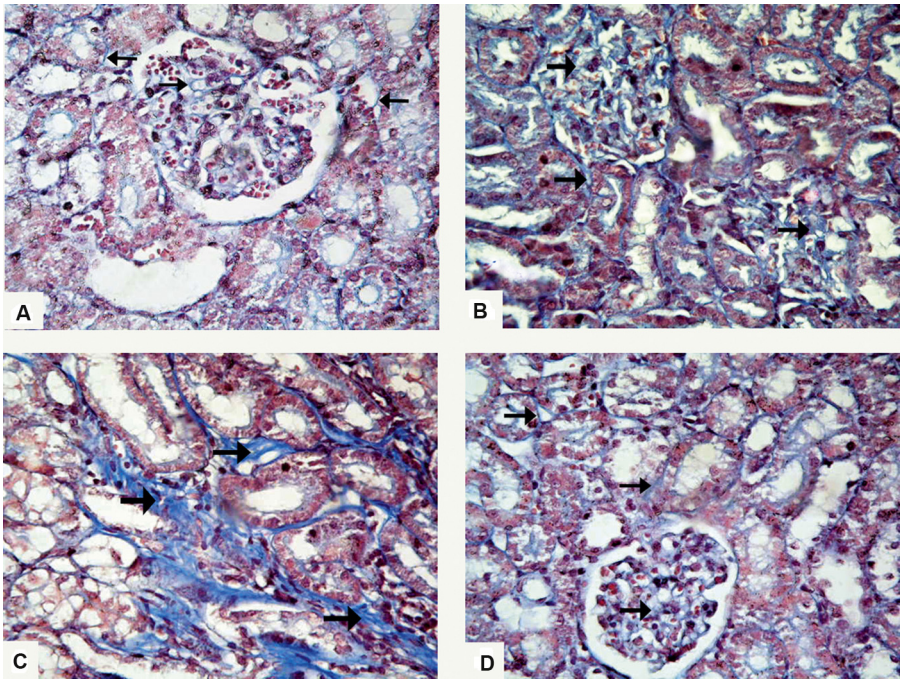

Fig. 5. Photomicrographs of renal sections stained with Masson's trichrome stain 400×. (A) Section from Group I (control group) shows normal distribution of collagen fibers (arrows) in the renal corpuscle and between the renal tubules. (B) In Group II (Adriamycin group), there is marked deposition of collagen fibers among glomerular capillaries and between the renal tubules (arrows), and (C) peritubular collagen deposition (arrows). (D) Renal cortex of Group III (granulocyte-colony-stimulating-factor group) shows mild deposition of collagen fibers in the renal corpuscle and between renal tubules (arrows).

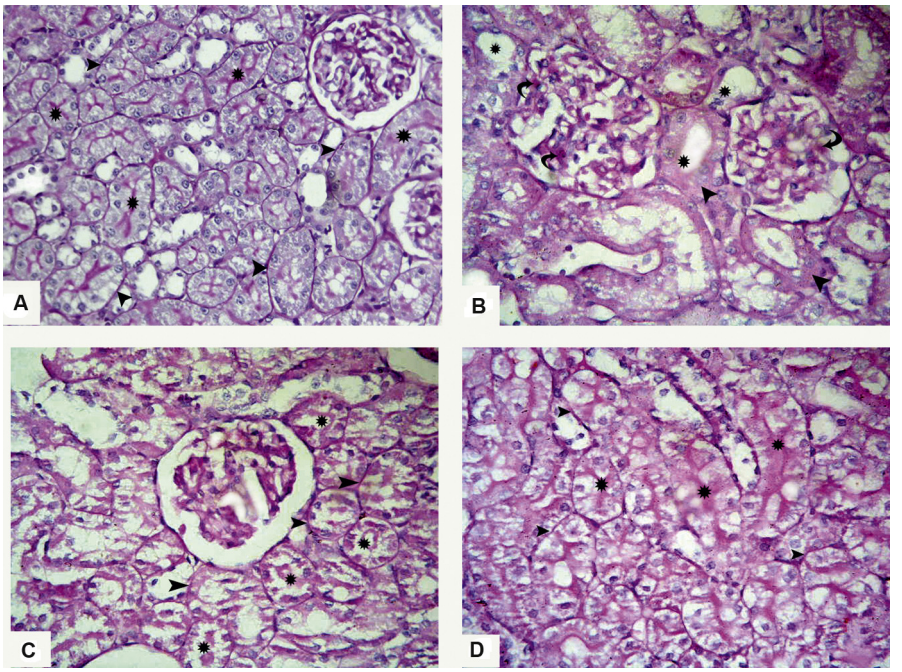

Fig. 6. Photomicrographs of sections stained with periodic acid–Schiff stain 400×. (A) Renal cortex of Group I (control group) shows many cortical tubules with intact brush border (asterisks) and clear basal laminae (arrowheads). (B) Section from Group II (Adriamycin group) shows partial or complete loss of brush border in most of the tubules (asterisks), the tubular basal laminae are interrupted at many sites (arrowheads), and the renal corpuscles show expanded periodic acid–Schiff +ve mesangium (curved arrows). (C, D) Renal sections from Group III (granulocyte-colony-stimulating-factor group) show many cortical tubules with preserved brush border (asterisks); also, continuous clear basal laminae (arrowheads) are detected in nearly all the tubules.

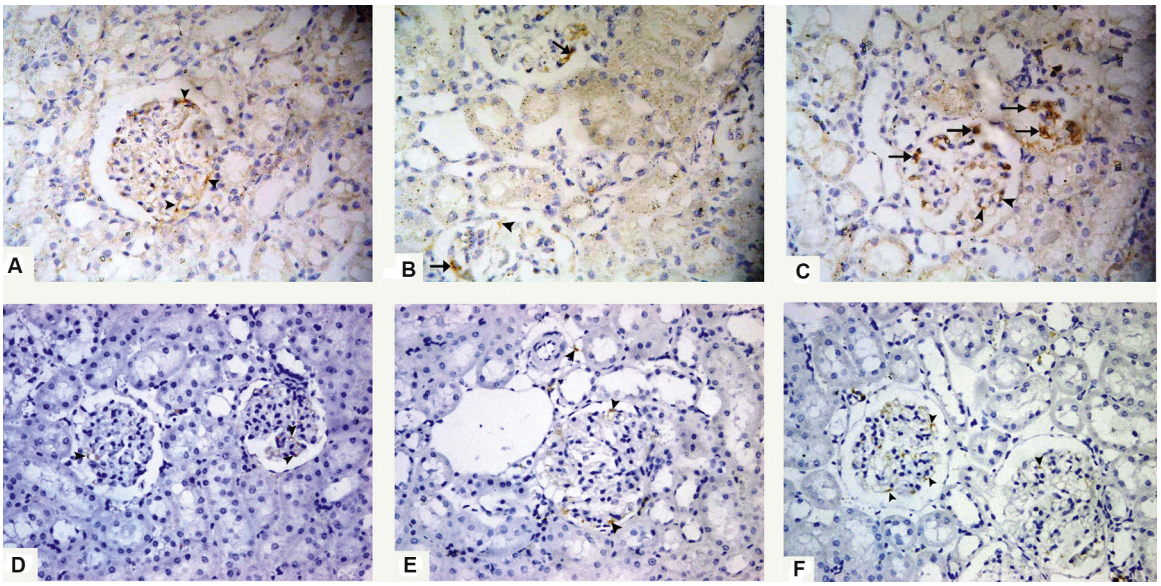

Fig. 7. Photomicrographs of renal sections stained with anti-CD34 antibody 400×. (A) Group I (control group) on Day 5 shows positive immunoreactivity in the endothelial cells only (arrowheads), and no immunopositive hematopoietic stem cells can be detected. (B) Group II (Adriamycin group) on Day 5 shows few immunopositive hematopoietic stem cells within the renal glomeruli (arrows). Immunoreaction can be also detected in the endothelial cells (arrowhead). (C) Renal cortex of Group III (granulocyte-colony-stimulating-factor group) on Day 5 shows many immunopositive hematopoietic stem cells within the renal glomeruli (arrows). They appear as small cells with brown cytoplasmic reaction and small rounded nuclei. Immunoreaction can be also detected in the endothelial cells (arrowheads). (D) Renal cortex of Group I (control group) after 6 weeks showing positive immunoreactivity in the endothelial cells only (arrowheads). (E) Group II (Adriamycin group) after 6 weeks shows positive immunoreaction in the endothelial cells only (arrowheads). No immunopositive hematopoietic stem cells can be detected. (F) A section from Group III (granulocyte-colony-stimulating-factor group) after 6 weeks shows positive immunoreaction only in the endothelial cells (arrowheads). No immunopositive hematopoietic stem cells can be detected.

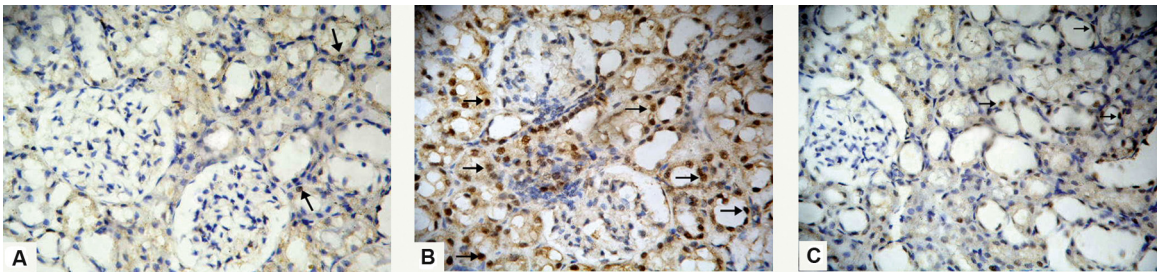

Fig. 8. Photomicrographs of sections stained with anticaspase-3 antibody 400×. (A) Group I (control group) shows scarce solitary nuclear immunoreactivity for caspase-3 in the renal tubules (arrows). (B) Renal tubular cells in sections of Group II (Adriamycin group) show widespread nuclear immunoreactivity for caspase-3 (arrows). (C) In Group III (granulocyte-colony-stimulating-factor group), some tubular cells show brown nuclear immunoreaction for caspase-3 (arrows).

border and clear basal laminae (Figure 6A). Sections in the renal cortex from the ADR group showed partial or complete loss of the brush border in most of the tubules. The tubular basal laminae were interrupted at many sites. The renal corpuscles showed expanded PAS +ve mesangium (Figure 6B). Sections from the G-CSF group revealed many cortical tubules with preserved brush border, and continuous clear basal laminae were detected in nearly all the tubules (Figures 6C and 6D).

3.4. Immunohistochemical stains

3.4.1. CD34-immunostained sections

On Day 5, positive immunoreactivity in the control group appeared only in the endothelial cells. No immunopositive HSCs could be detected (Figure 7A). As for Group II (ADR group), few immunopositive HSCs were seen within the glomeruli. An immunoreaction could be detected in the endothelial cells (Figure 7B), whereas in Group III (G-CSF group) many immunopositive HSCs were seen within the glomeruli. They appeared as small cells showing brown cytoplasmic reaction and small rounded nuclei. An immunoreaction could be detected in the endothelial cells (Figure 7C).

After 6 weeks, sections from all groups (I–III) showed positive immunoreactivity only in the endothelial cells. No immunopositive HSCs could be detected (Figures 7D–7F).

3.4.2. Caspase-3-immunostained sections

Sections from both control subgroups (IA and IB) showed scarce nuclear immunoreactivity for caspase-3 in the renal tubules (Figure 8A). Regarding sections from the

Table 2
Morphometric results of the experimental groups ± standard deviation.

	Group I (control)	Group II (ADR)	Group III (G-CSF)
Mean number of affected renal corpuscles	0.50 ± 0.10	8.0 ± 2.40 [a]	3.0 ± 1.15
Mean area % of collagen fibers	9.44 ± 3.08	21.22 ± 5.67 [a]	12.85 ± 2.81
Mean optical density of PAS +ve reaction	1.80 ± 0.20	0.43 ± 0.12 [b]	1.05 ± 0.53 [c]
Mean number of CD34-immunopositive HSCs on Day 5	0.00 ± 0.00	2.10 ± 0.99 [b]	7.0 ± 2.40 [d]
Mean number of CD34-immunopositive HSCs after 6 wks	0.00 ± 0.00	0.00 ± 0.00 [e]	0.00 ± 0.00 [e]
Mean number of caspase-3-immunopositive cells	4.0 ± 1.0	36.50 ± 6.11 [a]	12.10 ± 2.72 [b]

[a] Significant increase compared to Groups I and III.
[b] Significant decrease compared to Group I.
[c] Significant increase compared to Group II.
[d] Significant increase compared to Groups I and II on the same day.
[e] Significant decrease compared to the same groups on Day 5.
ADR = Adriamycin; G-CSF = granulocyte colony-stimulating factor; HSC = hematopoietic stem cell; PAS = periodic acid–Schiff.

ADR group, there was widespread caspase-3 immunoreactivity that appeared as a brown nuclear reaction in the renal tubules (Figure 8B). The examined sections from the G-CSF group showed few renal tubular cells exhibiting a brown nuclear reaction (Figure 8C).

3.5. Morphometric results

Morphometric results are illustrated in Table 2.

4. Discussion

Numbers of prevalent CKD patients continue to rise, and as this occurs, nephrologists are confronted with the development of new protective approaches for the complex medical problems unique to these patients [13]. That is why the present study was done to investigate the protective effect of enhanced mobilization of HSCs by G-CSF in a rat model of nephropathy. ADR was chosen to induce nephropathy, as it was reported to induce renal injury in rodents similar to that occurred in humans. It is characterized by rapid onset of glomerular damage and proteinuria, which progresses to segmental sclerosis, in addition to tubulo-interstitial damage and scar formation [14].

In the current study, the mobilization of endogenous HSCs was enhanced by the administration of G-CSF for 5 consecutive days. It was previously declared that administration of G-CSF daily for 4–6 days resulted in a 10–30-fold increase in the number of circulating stem cells [15]. The mobilization and homing of HSCs in the renal tissue were assessed immunohistochemically using CD34 on the 5th day, the day of maximum HSC mobilization [16], and at the end of the experiment (after 6 weeks) [2]. The effectiveness of G-CSF therapy was evaluated using serological, histological, and morphometric studies.

The measurement of BUN and serum-creatinine levels is regarded as a reliable indicator for the assessment of kidney functions [17]. In the present work, BUN and serum-creatinine levels showed a significant elevation in both Groups II (ADR group) and III (G-CSF group) as compared to the control, 6 weeks after a single dose of intravenous ADR, which confirms the occurrence of renal dysfunction. Similarly, other researchers reported a significant increase in both parameters after a single injection of ADR in rats [18]. It was proved that the oxidant injury caused by ADR via reactive-oxygen-species (ROS) production augments urea and creatinine levels in serum and albumin excretion in urine [19]. However, Group III showed a significant decrease in BUN and serum-creatinine levels as compared to the ADR group, suggesting that G-CSF could exert a protective effect against ROS and preserve renal functions.

The current study revealed various degenerative changes in renal corpuscles, and cortical and medullary tubules in sections from Group II (ADR group). There was partial to complete destruction of a large number of renal corpuscles with loss of glomerular capillary tufts. This was confirmed by morphometry, which revealed a significant increase in the number of affected renal corpuscles when compared to the control. Marked glomerular capillary-tuft distortion or complete loss was described in case of severe renal injury [20]. Also, the present research showed severe tubular damage; the lining tubular epithelial cells exhibited vacuolated cytoplasm and pyknotic nuclei together with desquamation and shedding of epithelial cells. Tubular dilatation with intraluminal dense acidophilic hyaline casts, capillary congestion, marked interstitial hemorrhage, and mononuclear cellular infiltration were also evident. All these findings were confirmed by toluidine-blue sections that revealed tubular cytoplasmic vacuolation, nonclear basal striations, partial or complete loss of brush border, epithelial desquamation, interrupted basal laminae, as well as small irregular nuclei in most renal tubules.

These results were consistent with Zickri et al. [5] who demonstrated that a single intravenous injection of ADR in rats resulted in a tubulo-interstitial injury in the form of vacuolated cytoplasm, dark nuclei in the cells lining most tubules, detached epithelial cells, and desquamated dark nuclei in the lumina of some tubules. It was postulated that ADR-induced tubular atrophy may be related to the formation of reactive metabolites that attack cell membranes and result in peroxidation of polyunsaturated fatty acids. Damaged cell membranes resulted in the detachment of tubular epithelium and desquamation of the nuclei into the lumen [21]. The intratubular hyaline casts might represent cellular debris that underwent molecular changes. The cells and their debris that detach from the tubular basement membrane combine with proteins present in the tubular lumen, such as Tamm–Horsfall protein, resulting in cast formation. Furthermore, impaired sodium reabsorption, by injured

tubular epithelium, results in increased sodium concentration in the tubular lumina. This causes polymerization of Tamm–Horsfall protein forming gel and contributing to cast formation [22].

Regarding vascular alterations, other investigators reported that intravenous ADR in rats resulted in expanded and congested renal tubular capillaries with inflammatory infiltration [18,23]. It was stated that, in ADR-induced nephrosis, cell infiltration is a hallmark that preceded the development of tubular cell atrophy [24]. This inflammatory response results from the oxidative stress caused by ADR and leads to vascular congestion, which reduces the ability to clear toxic radicals [25].

Masson's trichrome stain was used in this work to detect fibrosis. Sections from the ADR group revealed marked deposition of collagen within the glomeruli, as well as between renal tubules. This was supported by a morphometric analysis, where the mean area percent of collagen fibers was significantly higher than the control. Likewise, it was documented that ADR-induced renal injury in rats resulted in severe interstitial fibrosis [2]. In fact, a variety of inflammatory cells and growth factors/chemokines participate in renal interstitial fibrosis as transforming growth factor-beta 1 (TGF-β1), which plays an important role in the induction of myofibroblasts responsible for the production of extracellular matrices, such as collagen and fibronectin. TGF-β1 is produced mainly by macrophages, together with platelet-derived growth factor and tumor necrosis factor-α, and both induce the conversion of interstitial cells into myofibroblasts with subsequent deposition of collagen [26].

Assessing brush-border preservation in proximal tubules is a highly sensitive marker for monitoring the survival and function of proximal tubular cells [27]. PAS-stained sections from the ADR group showed partial to complete loss of brush border in most tubules, and the basal laminae were interrupted at some sites. Also, the renal corpuscles showed expanded PAS +ve mesangium. Statistically, there was a significant decrease in the optical density of PAS +ve reaction in ADR compared to the control. This was consistent with other authors who reported marked tubular epithelial injury after intravenous ADR in rats, manifested by loss of tubular brush border and expansion of the mesangium [12]. This could be clarified by the fact that ROS production during ADR-induced nephrosis resulted in the rapid loss of cytoskeletal integrity, which led to the loss of brush-border microvilli, cell junctions, and loss of polarity with mislocalization of adhesion molecules and other membrane proteins, such as the Na^+K^+-ATPase and β-integrins [28].

Concerning sections from Group II (ADR group) stained with anticaspase-3 antibody, there was widespread positive immunoreactivity in the renal tubules indicating abundant apoptotic cells. This was confirmed by morphometry that proved a significant increase in the number of caspase-3-positive cells when compared to the control. This is consistent with Chen et al. [29] who reported augmented apoptosis in the renal tubular cells in ADR-treated rats. It was suggested that renal apoptosis is associated with overexpression of inducible nitric oxide synthase, heat shock protein 60, and hypoxia-inducible factor-1α molecules involved in the context of renal hypoxia and cell stress response in progressive renal disease induced by ADR [30].

Renal sections stained with anti-CD34 antibody from the ADR group showed few immunopositive HSCs within the glomeruli on Day 5. It was reported that, in animals that underwent ADR-induced kidney injury, anti-CD34 immunostaining revealed the presence of few CD34 +ve cells in kidney specimens within a few days from its injection [31]. By contrast, sections from the G-CSF group revealed a large number of CD34-immunopositive HSCs on Day 5, which was significantly higher than the control and ADR groups. This indicates that G-CSF could efficiently mobilize HSCs from BM and increase their homing to the injured renal cells. Similar results were obtained by Modelli de Andrade et al. [2] who reported that CD34 expression increased in the group treated with G-CSF. However, after 6 weeks, no immunopositive HSCs could be detected in both glomeruli and renal tubules, suggesting their differentiation. When HSCs differentiate, they lose the CD34 marker and acquire other biochemical markers specific to a lineage [32].

Preservation of renal structure was found in sections from Group III (G-CSF group) with features of less severe injury than the ADR group, as most renal corpuscles appeared normal with intact glomerular tufts. This was established by morphometry that proved a significant decrease in the number of affected renal corpuscles as compared to the ADR group. Nearly all tubular cells showed vesicular nuclei, except for mild peritubular capillary congestion with mild cytoplasmic vacuolation of some areas of tubular cells. In addition, the toluidine-blue semithin sections showed clear basal striations, prominent brush border, and large vesicular nuclei in most renal tubules. Similarly, other studies reported a reduced number of atrophic sites (glomerular atrophy + tubular atrophy + inflammatory infiltrate) in the G-CSF-treated mice after ADR-induced nephropathy [2]. It was postulated that enhanced mobilization of adult HSCs and endothelial progenitor cells from the BM by G-CSF was responsible for the lesser degree of tissue damage in diseased animals as compared to controls through transdifferentiation and trophic effects by producing different growth factors [33,34].

Masson's trichrome-stained sections from the G-CSF group showed mild deposition of collagen fibers in renal corpuscles and between renal tubules. Statistically, the mean area percent of collagen fibers was significantly lower when compared to the ADR group. This was in accordance with Fang et al. [35] who found that G-CSF treatment significantly reduced carbon dichloride- and pentachloride-induced kidney damage and collagen deposition in mice. The antifibrotic effect of G-CSF is multifactorial. First, G-CSF-mobilized HSCs alter the microenvironment by producing interleukin-10, an antifibrogenic cytokine, or antagonists of tumor necrosis factor-α that disrupt signaling pathways leading to fibrosis [36]. Secondly, G-CSF reduces serum levels of TGF-β1, which promotes the fibrogenic response of the interstitial cells. Third, G-CSF-mobilized HSCs prevent activated cells from secreting TGF-β1 [37].

The examined PAS-stained sections from the G-CSF group revealed that most cortical tubules had preserved brush borders and continuous basal laminae. The morphometric analysis proved a statistically significant increase in the optical density of PAS +ve reaction in the G-CSF group when compared to the ADR group. It was stated that the administration of G-CSF preserves the tubular brush border and ameliorates tubular necrosis, suggesting its protective effect on the cytoskeletal integrity of renal tubular cells [38].

As regards caspase-3-immunostained sections from the G-CSF group, there were few renal tubular cells exhibiting positive nuclear immunoreactivity indicating mild apoptosis. This was established by the morphometric analysis that showed a significant decrease in the number of caspase-3-positive cells compared to the ADR group. In addition, it was demonstrated that mice treated with G-CSF had significantly lower numbers of apoptotic renal tubular epithelial cells (RTECs) compared to untreated mice [39]. This might suggest the antiapoptotic effect of G-CSF on RTECs. The antiapoptotic effect of G-CSF on RTECs could be explained by the following: (1) the activation of Janus kinase/signal transducer and activator of the transcription signaling pathway through the G-CSF receptor on RTECs [40]; (2) G-CSF stimulates angiogenesis, which promotes functional recovery of damaged tissue based on the fact that mobilized HSCs can differentiate into vascular endothelium and vascular smooth muscles [41]; and (3) G-CSF indirectly affects RTEC function via the production of hepatocyte growth factor, a potent renotrophic factor with mitogenic and antiapoptotic activities on RTECs [39].

5. Conclusions

G-CSF proved to have a potential renoprotective capacity at both morphological and functional levels. It could stimulate the regenerative process through multiple direct and indirect actions, such as enhancing endogenous BM HSC mobilization and homing to the injured kidney, reduction of collagen deposition, and inhibition of RTEC apoptosis. If the renoprotective role of G-CSF is proven to be efficient in humans, it will represent a perfect choice for CKD patients protecting them from reaching end stages that need dialysis or kidney transplantation.

Conflicts of interest

The authors have no conflicts of interest to declare.

References

[1] Jha V, Garcia-Garcia G, Iseki K, Li Z, Naicker S, Plattner B, et al. Chronic kidney disease: global dimension and perspectives. Lancet 2013;382:260–72.

[2] Modelli de Andrade LG, Viero RM, Cordeiro de Carvalho MF. Treatment of Adriamycin-induced nephropathy with erythropoietin and G-CSF. J Nephrol 2013;26:534–9.

[3] Zhu XY, Lerman A, Lerman LO. Mesenchymal stem cell treatment for ischemic kidney disease. Stem Cells 2013;31:1731–6.

[4] Hopkins C, Li J, Rae F, Little MH. Stem cell options for kidney disease. J Pathol 2009;217:265–81.

[5] Zickri MB, Zaghloul S, Farouk M, Abdel Fattah MM. Effect of stem cell therapy on Adriamycin induced tubulointerstitial injury. Int J Stem Cells 2012;5:130–9.

[6] Prakash A, Chopra K, Medhi B. Granulocyte-colony stimulating factor improves Parkinson's disease associated with co-morbid depression: an experimental exploratory study. Indian J Pharmacol 2013;45:612–5.

[7] Ozmen J, Bobryshev Y, Lord R. Identification of dendritic cells in aortic atherosclerotic lesions in rats with diet-induced hypercholesterolaemia. Histol Histopathol 2002;17:223–37.

[8] Bancroft J, Cook H. Immunocytochemistry. Manual of histological techniques and their diagnostic applications. 2nd ed Edinburgh/London/Madrid/Melbourne/New York/Tokyo: Churchill Livingstone; 1994. p. 263–325.

[9] Kiernan J. Histological and histochemical methods: theory and practice. 3rd ed London/New York/New Delhi: Arnold Publishers; 2001. p. 111–62.

[10] Kamada S, Kikkawa U, Tsujimoto Y, Hunter T. Nuclear translocation of caspase-3 is dependent on its proteolytic activation and recognition of a substrate-like protein(s). J Biol Chem 2005;280:857–60.

[11] Hayat MR. Basic techniques for transmission electron microscopy. 1st ed New York: Academic Press; 1986. p. 1–10.

[12] Wang Y, Wang YP, Tay YC, Harris DC. Progressive Adriamycin nephropathy in mice: sequence of histologic and immunohistochemical events. Kidney Int 2000;58:1797–804.

[13] Thomas R, Kanso A, Sedor JR. Chronic kidney disease and its complications. Prim Care Clin Office Pract 2008;35:329–44.

[14] Turnberg D, Lewis M, Moss J, Xu Y, Botto M, Cook HT. Complement activation contributes to both glomerular and tubulointerstitial damage in Adriamycin nephropathy in mice. J Immunol 2006;177:4094–102.

[15] Jin P, Wang E, Ren J, Childs R, Shin JW, Khuu H, et al. Differentiation of two types of mobilized peripheral blood stem cells by microRNA and cDNA expression analysis. J Transl Med 2008;6:39–50.

[16] Waller CF, Bronchud M, Mair S, Challand R. Comparison of the pharmacodynamic profiles of a biosimilar filgrastim and Amgen filgrastim: results from a randomized, phase I trial. Ann Hematol 2010;89:971–8.

[17] Salgado JV, Neves FA, Bastos MG, Franca AK, Brito DJ, Santos EM, et al. Monitoring renal function: measured and estimated glomerular filteration rates—a review. Braz J Med Biol Res 2010;43:528–36.

[18] Ding ZH, Xu ML, Wang SZ, Kou JQ, Xu YL, Chen CX, et al. Ameliorating Adriamycin-induced chronic kidney disease in rats by orally administrated cardiotoxin from *Naja naja atra* venom. Evid Based Complement Alternat Med 2014;62:1–10.

[19] Abo-Salem OM, El-Edel RH, Harisa GE, El-Halawany N, Ghonaim MM. Experimental diabetic nephropathy can be prevented by propolis: effect on metabolic disturbances and renal oxidative parameters. Pak J Pharm Sci 2009;22:205–10.

[20] Klatt EC. Robbins and Cotran atlas of pathology. Toronto, Canada: Saunders Elsevier; 2006. p. 318–60.

[21] Ayla S, Seckin I, Tanriverdi G, Cengiz M, Eser M, Soner BC, et al. Doxorubicin induced nephrotoxicity: protective effect of nicotinamide. Int J Cell Biol 2011;13:495–510.

[22] Abuelo GJ. Current concepts: normotensive ischemic acute renal failure. Engl J Med 2007;357:797–805.

[23] Ning H, Wu H, Tian X, Guo Y, Shen W, Wang X, et al. Effects of carpio decoction on the structure of kidney in rats with Adriamycin-induced nephrosis. Food Nutr Sci 2013;4:124–30.

[24] Mihailovic-Stanojevic N, Jovovic D, Miloradovic Z, Grujic-Milanovic J, Jerkic M, Markovic-Lipkovski J. Reduced progression of Adriamycin nephropathy in spontaneously hypertensive rats treated by losartan. Nephrol Dial Transplant 2009;24:1142–50.

[25] Sutton TA. Alteration of microvascular permeability in acute kidney injury. Microvasc Res 2009;77:4–7.

[26] Farris AB, Colvin RB. Renal interstitial fibrosis: mechanisms and evaluation. Curr Opin Nephrol Hypertens 2012;21:289–300.

[27] Lange C, Togel F, Ittrich H, Clayton F, Nolte-Ernsting C, Zander AR, et al. Administered mesenchymal stem cells enhance recovery from ischemia/reperfusion-induced acute renal failure in rats. Kidney Int 2005;68:1613–7.

[28] Bonventre JV, Yang L. Cellular pathophysiology of ischemic acute kidney injury. J Clin Invest 2011;121:4210–21.

[29] Chen CH, Lin H, Hsu YH, Sue YM, Cheng TH, Chan B, et al. The protective effect of prostacyclin on Adriamycin-induced apoptosis in rat renal tubular cells. Eur J Pharmacol 2012;529:8–15.

[30] Stoyanoff TR, Todaro JS, Aguirre MV, Brandan NC. Cell stress, hypoxic response and apoptosis in murine Adriamycin induced nephropathy. J Pharmacol Toxicol 2012;7:344–58.

[31] Mark A, Sun Z, Warren D, Lonze B, Knabel M, Williams G, et al. Stem cell mobilization is life saving in an animal model of Adriamycin induced nephropathy. Ann Surg 2010;252:591–6.

[32] Devine H, Tierney K, Schmit-Pokorny K, McDermott K. Mobilization of hematopoietic stem cells for use in autologous transplantation. Clin J Oncol Nurs 2010;2:212–22.
[33] Zhang JJ, Yi ZW, Dang XQ, He XJ, Wu XC. Mobilization effects of SCF along with G-CSF on bone marrow stem cells and endothelial progenitor cells in rats with unilateral ureteral obstruction. Zhongguo Dang Dai Er Ke Za Zhi 2007;9:144–8.
[34] Stokman G, Leemans JC, Stroo I. Enhanced mobilization of bone marrow cells does not ameliorate renal fibrosis. Nephrol Dial Transplant 2008;23:483–91.
[35] Fang B, Luo S, Song Y, Li N, Li H, Zhao R. Intermittent dosing of G-CSF to ameliorate carbon tetrachloride-induced kidney fibrosis in mice. Toxicology 2010;270:43–8.
[36] Tilg H, Jalan R, Kaser A, Davies NA, Offner FA, Hodges SJ, et al. Anti-tumor necrosis factor alpha monoclonal antibody therapy in severe alcoholic hepatitis. J. Hepatol 2003;38:419–25.
[37] Li N, Zhang L, Li H, Fang B. Administration of granulocyte colony-stimulating factor ameliorates radiation-induced hepatic fibrosis in mice. Transplant Proc 2010;42:3833–9.
[38] Nafar M, Parvin M, Sadeghi P, Ghoraishian M, Soleimani M, Tabibi A, et al. Effects of stem cells and granulocyte colony stimulating factor on reperfusion injury. Iran J Kidney Dis 2010;4:207–13.
[39] Nishida M, Hamaoka K. How does G-CSF act on the kidney during acute tubular injury? Nephron Exp Nephrol 2006;104:e123–8.
[40] Harada M, Qin Y, Takano H, Minamino T, Zou Y, Toko H, et al. G-CSF prevents cardiac remodeling after myocardial infarction by activating the Jak-Stat pathway in cardiomyocytes. Nat Med 2005;11:305–11.
[41] Ohki Y, Heissig B, Sato Y, Akiyama H, Zhu Z, Hicklin DJ, et al. Granulocyte colony-stimulating factor promotes neovascularization by releasing vascular endothelial growth factor from neutrophils. FASEB J 2005;19:2005–7.